Experimental analysis of the flow field on a hammerhead fairing satellite launch vehicle in transonic regime using Pressure Sensitive Paint (PSP)

Ana Cristina Avelar[1], João Batista P. Falcão Filho[2], Josenei G. Medeiros[3], Geovanny M. Romero[4]
[1]Atmospheric Science Division, Institute of Aeronautics and Space, São José dos Campos, Brazil
[2]Aerodynamics Division, Institute of Aeronautics and Space,São José dos Campos, Brazil
[3,4]Technological Institute of Aeronautics, São José dos Campos, Brazil

*corresponding author: anacristina.avelar@gmail.com

Abstract The purpose of the present study is to analyze experimentally the flow patterns on the frontal part of a hammerhead-type fairing launcher vehicle, which is the Brazilian Satellite Launch Vehicle (VLS-1). The wind tunnel model was based on the dimensions of the VLS-1, and built on a scale 1:37. The region studied is characterized by three distinct sections: a rounded tip followed by a frustum cone, a constant diameter segment for the satellite compartment, a boat-tail shape sector to adjust the geometry to the following stage, and a limited length of this last propulsive stage of the vehicle. The effects of geometry changes of the boat-tail sector on the pressure field over the model are analyzed for different Mach number values, 0.6, 0.8 and 1.0. The experiments were conducted in the Pilot Transonic Wind Tunnel (TTP), which is located in São José dos Campos, at the Institute of Aeronautics and Space (IAE) and the technique of Pressure Sensitive Paint (PSP) was used for obtaining pressure fields over the model. The results obtained show that the variation of the boat tail angle has a significant effect on the pressure distribution over the region analyzed.
Keywords: VLS, Transonic Wind Tunnel, Hammerhead-type fairing, Pressure Sensitive Paint (PSP)

1 Introduction

In spite of being of non-conventional shape, the hammerhead-type fairing is rather common on satellite launchers vehicle because of the demand to accommodate spacecraft with a diameter larger than the last boosting stage [1], as well to protect the payload, a satellite, inside it from aerodynamic and heating loads [2]. This is the case of the first Brazilian Satellite Launch Vehicle (VLS), Fig.1, which is of the cluster type with four strap-on boosters around the central core [2]. The VLS has a length of 19 meter, a total mass of 50 tons and a thrust of 100kN, allowing to place in circular orbits satellites weighting from 100kg to 350kg at altitudes ranging from 250 km to 1000 km [3].

Fig.1 The VLS Vehicle geometry representation.

The VLS-1 vehicle complex aerodynamic configuration resulted from the hammerhead-type fairing and the booster assembly may bring significant problems due to the complex flow phenomena taking place, mainly at transonic speeds [2]. For this reason, VLS models have being already intensively tested in wind tunnel for evaluating both the aerodynamics performance of the actual geometry, in the design phase, and also for numerical code validation purposes. Actually, great effort in research, both numerically and experimentally, have already been spent in order to investigate several VLS characteristics with the purpose of guaranteeing a good flight performance of the vehicle. Wind tunnel tests covering a wide range of test parameters such as Mach number, Reynolds number, and angle of incidence has already been conducted. In fact, due to the complicated geometry of the VLS vehicle, which makes necessary numerical flow simulations through well-validated codes, wind tunnels tests are of great importance. High-speed wind tunnel tests with 1/15th and 1/30th scale models are reported in [1]. The tests conducted included pressure measurements along the fairing

surface with variation of Mach number in the transonic range and flow visualization using *Schlieren* and oil flow techniques. In these tests, it was verified that the static pressure along the fairing presents significant variations, with different types of distribution. In fact, the hammerhead-type payload shroud, in which the maximum diameter of the fairing exceeds the diameter of the uppermost stage of the rocket, as schematically represented in Fig. 2, is a configuration that tends to flow separation during the transonic or supersonic flight regimes. Consequently, higher structural loads may occur over this region.

An important aspect to be investigated in wind tunnel regarding the VLS, as well as any other hammerhead-type fairing, is the flow patterns over the region represented in Fig.2, which is subjected to high pressure gradients.

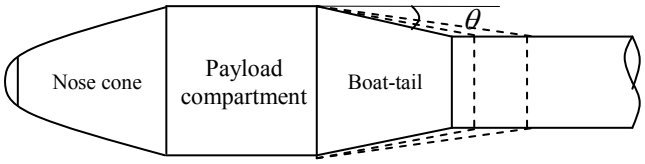

Fig. 2 Schematic representation a hammerhead shaped fairing.

In present paper, the influence of frustum cone angle, θ, an adapting boat-tail section, Fig. 2, called here as boat-tail angle, in a 1:37 scaled model of VLS-1, is investigated in a transonic wind tunnel for the Mach number values of 0.6, 0.8 and 1.0. The technique of Pressure Sensitive Paint (PSP) is used in this analysis. This technique is relatively new in comparison with the conventional methods and has the great advantage of high resolution, as well as the possibility to access any area of interest on the model surface. The PSP technique working principle is well documented in the literature [4, 5, 6] and it is based on an oxygen-quenching process in which excited molecules are deactivated by oxygen, this phenomenon produces different degrees of luminosity on the model surface. The PSP paint is composed of an oxygen-permeable polymer binder containing luminescent oxygen-sensitive molecules. When illuminated with light at an appropriate wavelength, the luminescent molecules become excited electronically to an elevated energy state. These molecules can decay to the ground state through a radioactive process, luminescence, or non-radioactive way through release of heat. In some materials, oxygen can interact with the luminescent molecules such that the change to the ground state can be non-radioactive, and takes place by colliding with an oxygen molecule, a process known as “oxygen quenching” [4]. A PSP system is composed of PSP paint, an illumination source, an image detector, and a long-pass filter. The PSP paint is distributed over the model surface and then illuminated by the excitation source making the PSP to luminescer. The luminescent intensity from the PSP is recorded by the detector and converted to pressure using a previously obtained calibration. The final pressure map is obtained using complex image processing techniques. A detailed description of this technique is given in [4].

2 Description of the Experiments

The experimental analysis reported in this paper was conducted in the Pilot Transonic Wind Tunnel (TTP), which is located in São José dos Campos, at the Institute of Aeronautics and Space (IAE). The tunnel has a test section that is 30 cm wide, 25 cm high and 80 cm length, with slotted walls to reduce shock reflection from the walls. The tunnel has a conventional closed circuit, continuously driven by a main compressor of 830kW of power, and with an intermittent injection system that operate in a combined mode, for at least 30 seconds. TTP has automatic pressure controls from 0.5 bars to 1.25 bars, with Mach number varying between 0.2 and 1.3 as well as control of temperature and humidity in its test section. In spite of the small size, the facility is very feasible to conduct tests with simplified geometry vehicles, quantitative tests of airplane basic configuration, tests in developing new aerodynamic transonic profiles and to perform basic and academic researches. A complete description of the TTP wind tunnel is presented in [7].

Fig. 3 TTP frontal view with the plenum chamber open.

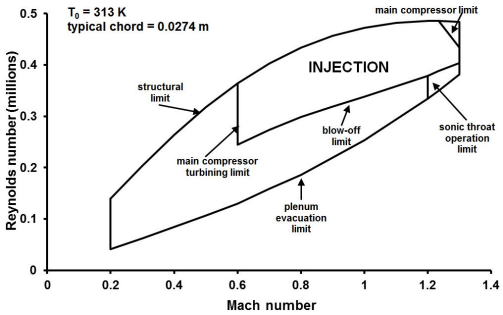

Fig. 4 TTP Operational envelope.

The tunnel has three sets of six multi-component internal balances for measuring forces and moments, ten modules of 16 pressure channels PSI (Pressure Sensitive Instrument) for pressure distribution tests, and has also a 2D probe positioning system, angle of attack remotely controlled system and re-entry flap capability.

The wind tunnel model was based on the dimensional specifications of the VLS-1 on a scale 1:37 to be fitted in TTP test section with a low blockage area ratio, 1.1%. In order to allow the use of different measurement techniques and to be easy to handle during geometric configuration changes, the model was constructed with four parts, as shown in Fig 5. The boat-tail is the interchangeable part of the assembly, with five different options for angles 4^o, 8^o, 16^o, 32^o and 90^o. The connections between the parts are made through screws. In the present study the configurations with 4^o, 16^o, 32^o and 90^o were considered.

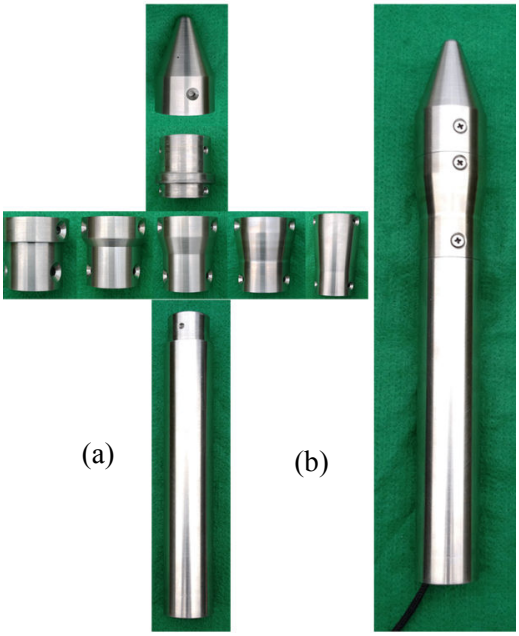

Fig. 5 VLS-1 model in scale 1:37. Fig.5a Model disassembled, showing all boat-tail section configurations, Fig.5b Model assembled for wind tunnel tests.

For the PSP measurements, acquisition and data processing, a commercial PSP system from Innovative Scientific Solutions, Inc. (ISSI) has been used. Images of the model painted with the PSP paint and installed in the TTP test section are shown in Fig. 6, Fig. 7 and Fig. 8. As it can be observed in Fig.8, vehicle nose has a 0.5 mm pressure tap to measure local pressure using a conventional pressure sensor for comparison with PSP results.

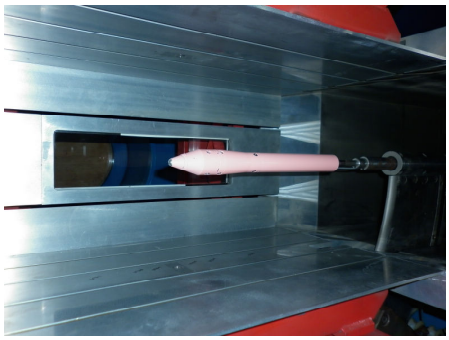

Fig. 6 Test model in TTP test section – lateral view.

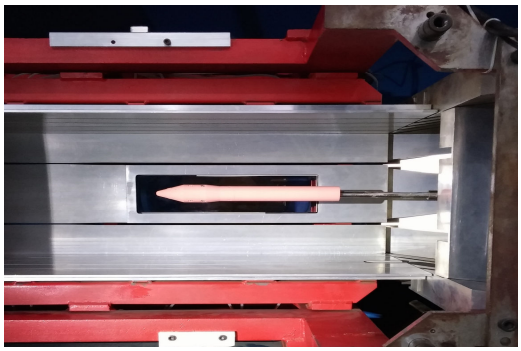

Fig. 7 Test model in TTP test section – frontal view.

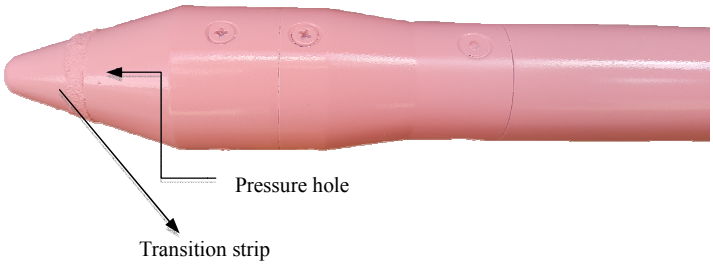

Fig. 8 Test model painted with the PSP paint.

In Fig. 8 it can be observed also that a transition strip was used to accelerate the laminar to turbulent boundary layer transition, simulating in this way a full Reynolds number condition [8].

3 Results and discussions

In this section, some of the preliminary results obtained up to now are going to be presented and discussed. Most of the PSP results are still being analyzed and will be presented further.

Initially it will be shown some results for the front model using 4 degrees of boat-tail angle, θ, or the fairing connecting the payload sector to the rocket engine. PSP results are shown as pressure distribution over the model using a color map from low values, represented in magenta to high values, represented in dark red. The corresponding graphic shows the pressure distribution along the centerline of the model with the streamwise coordinate made non-dimensional by the rocket diameter. A pressure tap at the model tip is used in all cases to adjust the PSP pressure curve level, as the pressure tap has higher precision.

Figure 9 presents the results obtained for free stream Mach number of 0.6, and θ of 4 degrees. At about 5% of the model length the transition strip disturbs the flow and consequently the pressure variation over the model. When it would be expected to have a small pressure decrease along the whole conical nose region, two distinct regions were formed: a large pressure increase before the transition strip, followed by a pressure drop due to its presence. This can be seen in the PSP image by the red region in the nose tip followed by the orange region. The pressure levels in both parts before and after the pressure strip indicate Mach numbers of 0.49 and 0.55, respectively. In general the result shows that the transition strip should be smaller to lessen its effect.

At the end of the cone and the initial part of the payload sector a significant pressure drop is observed. In this case the low pressure found indicates a Mach number of about 0.86, a value relatively high considering the freestream Mach number of 0.6. What comes from this point is more easily understood. The pressure is recovered in the cylindrical region of the payload sector, experiencing a small decrease because of the expansion caused by the boat-tail angle. As in a cone type sector it is expected a small pressure decrease, here in the boat-tail sector a small pressure increase is observed due to the diffuser effect undergone by the flow.

This increase is more significant at the end of the boat-tail sector by the change in the flow direction when the final cylindrical sector is reached. The pressure at the end of the model tends to freestream condition. The pressure value observed resulted in Mach number of 0.58, which is practically the freestream Mach number. It is interesting to observe a mild oscillation in the final region of the pressure distribution curve, which is still being investigated if it is related to the PSP technique or to physical disturbance of the flow.

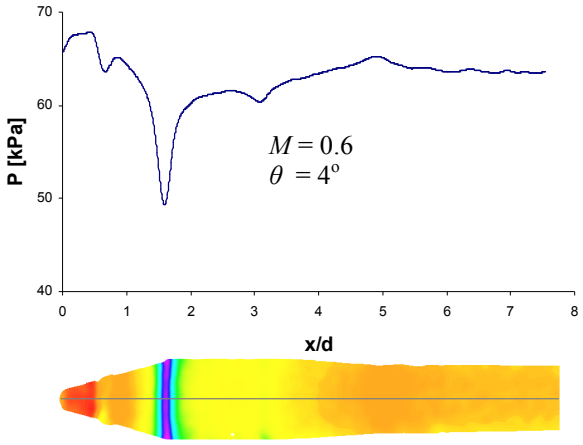

Fig. 9 PSP Results for $M = 0.6$ and $\theta = 4^{o}$.

Figure 10 shows the result for freestream Mach number of 0.8. The same aspects depicted in the previous case, for Mach number 0.6, can be observed. In this case the lowest pressure value at the beginning of the pay load sector indicates Mach number value of about 1.48. It is expected a shock-wave just after this supersonic region. In the PSP image it is possible to observe an enlargement of this expansion region. It is interesting to note the great acceleration produced by this type of nose, and concern about how the flow decelerates until reaching subsonic freestream condition is important to smooth the shock and expansion wave formations over the fuselage. This is provided by the boat-tail geometric shape as shown by this analysis.

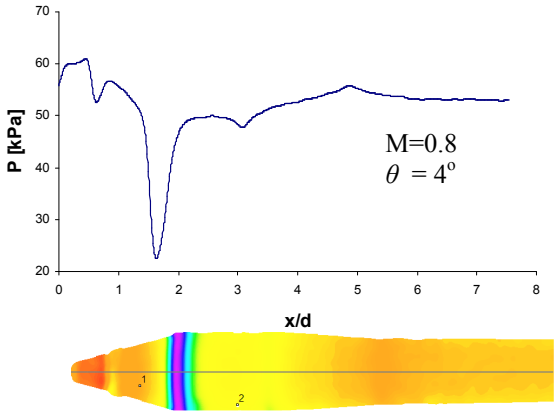

Fig. 10 PSP Results for $M = 0.8$ and $\theta = 4^{o}$.

A quite different result can be observed for the Mach number 1.0, Fig. 11. The lowest pressure value at the beginning of the payload sector indicates Mach number of 1.55, and it is followed by a complex and long shock-wave formation, reaching a final Mach number of 1.17 just followed by an expansion and reaching Mach number 1.26. From that point on, the pressure rises in two steps. In the first step the pressure rises probably because of compression waves formed to decelerate the flow and in the second step the final cylindrical part of the model acts creating another compression wave region. Because of the supersonic nature of the flow before these two steps the pressure will not converge to freestream condition but will reach pressure of about 14% higher than the freestream pressure, corresponding to a Mach number of about 0.89.

From this point on the subsonic region will accelerate until reaching freestream Mach number 1.0 condition.

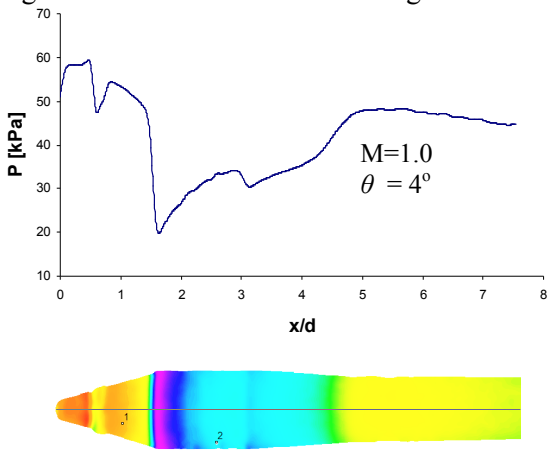

Fig. 11 PSP Results for $M = 1.0$ and $\theta = 4^{o}$.

Now the boat-tail is replaced by one with a boat tail angle of 16 degrees and the same test configurations were undertaken. It is interesting to observe in Fig. 12 that the PSP image in this case shows a green strip just in the beginning of the boat-tail sector. This can be seen in the graphic where it can be depicted pressure value resulting Mach number of 0.86. In this case, note how stable the pressure is in the payload sector. On the other hand, the pressure rises at the end of the boat-tail region, decelerating the flow because of the final cylindrical shape of the model, increasing the local pressure 5% above the freestream pressure value. From this point on the flow is gradually modified to freestream condition at the end of the model. It is worth note that this boat-tail angle cause a stronger decrease in the pressure compared to the last case. The Mach number at the end of the boat-tail was 0.71 compared to 0.64 from the last case.

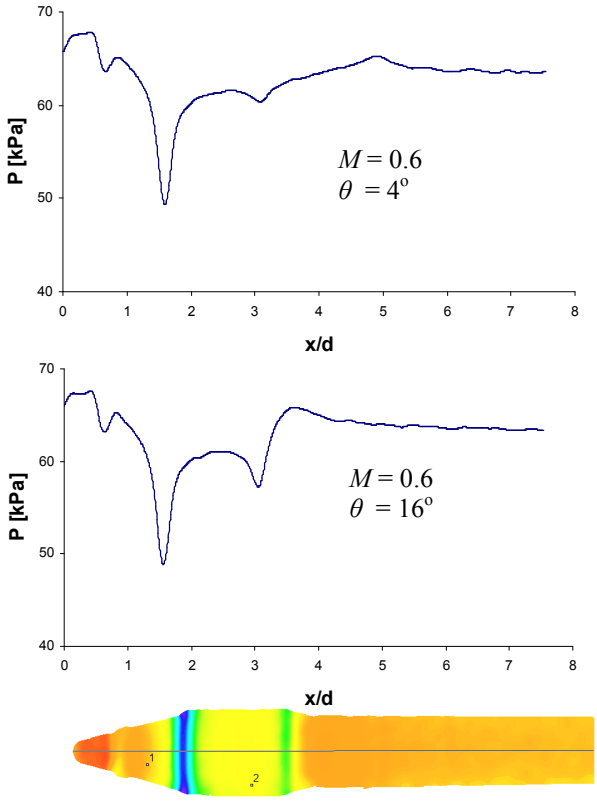

Fig. 12 PSP Results for $M = 0.6$ and $\theta = 16^{o}$.

When this region is investigated at freestream Mach number 0.8 case, the local condition is practically

critical, as can be seen in Fig. 13. It is interesting to observe also that the general aspect of the pressure distribution along the model surface in this case seems to have a better behavior. For example, the local pressure in the region of the payload sector is constant with local Mach number about 0.87.

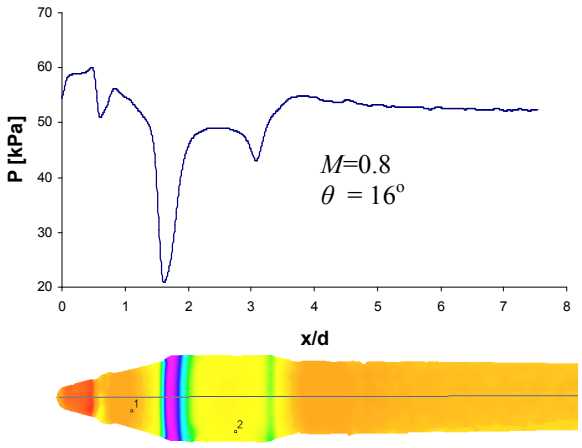

Fig. 13 PSP Results for $M = 0.8$ and $\theta = 16^{o}$.

However, for freestream Mach number 1.0 case, presented in Fig. 14, this geometry showed great variation of pressure along the model. The payload area suffers pressure variations from 18.1 kPa to 32.7 kPa and again to 18.7 kPa.

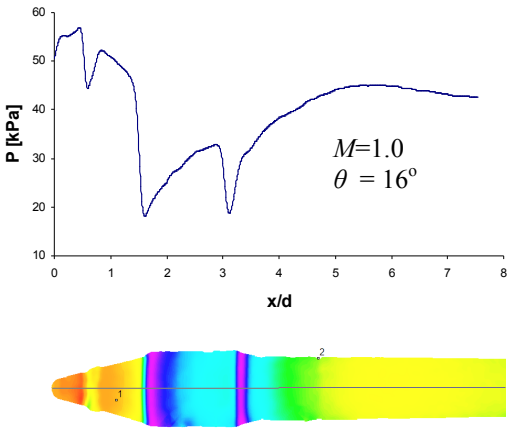

Fig. 14 PSP Results for $M = 1.0$ and $\theta = 16^{o}$.

Two more cases studied were for boat-tail angles of 32 degrees and 90 degrees to analyze the impact of the boat-tail angle increase. Figure 15 shows all the graphics of pressure profile for all boat-tail angles considered and all Mach number values. For $M = 0.6$ it is interesting to observe that the lowest pressure value obtained at the end of the boat-tail sector was observed for the boat-tail angle of 16 degrees, 57 kPa. For the other cases the local pressure was about 60 kPa. For Mach number 0.8 the pressure distribution along the model had practically the same aspect as for Mach number 0.6. The lowest local pressure at the end of the boat-tail was observed for boat-tail angle of 16 degrees, 43 kPa, whilst for the other geometries this value was about 48 kPa.

For Mach number 1.0 the pressure distribution along the model presented a significant difference from the subsonic cases. Again, and more noticeable, the lowest local pressure at the end of the boat-tail was observed for boat-tail of 16 degrees (19 kPa) and for the other geometries this value was about 28 kPa.

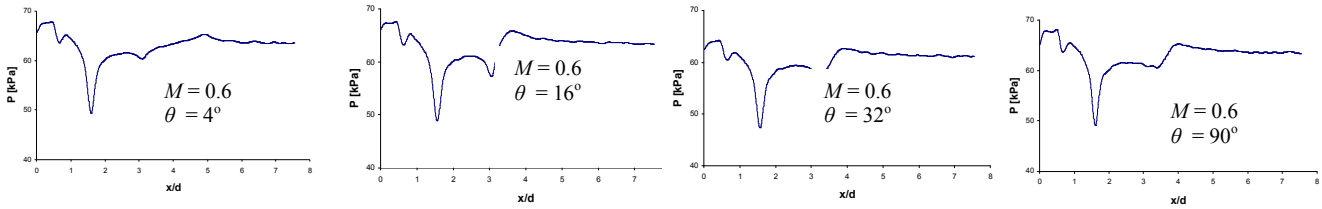

Fig. 15 PSP Profiles for $M = 0.6$ and θ equal to 4°, 16°, 32°, 90°.

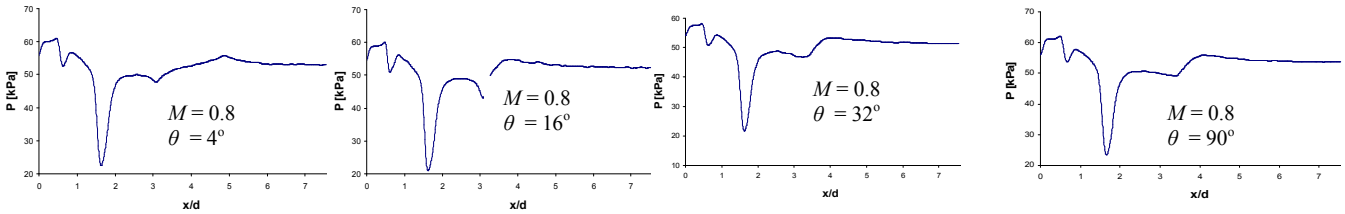

Fig. 16 PSP Profiles for $M = 0.8$ and θ equal to 4°, 16°, 32°, 90°.

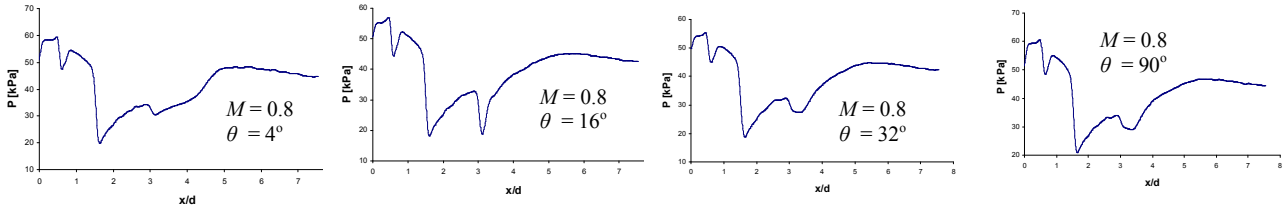

Fig. 16 PSP Profiles for $M = 0.8$ and θ equal to 4°, 16°, 32°, 90°.

By observing the PSP images of the four boat-tail geometry cases for Mach number 1.0 it is possible to realize the impact of the pressure decrease at the end of the boat-tail sector.

It is important to observe that the models are not the same length because of the boat-tail length. The magenta region at the end of the boat-tail clearly indicates this low value for boat-tail angle of 16 degrees.

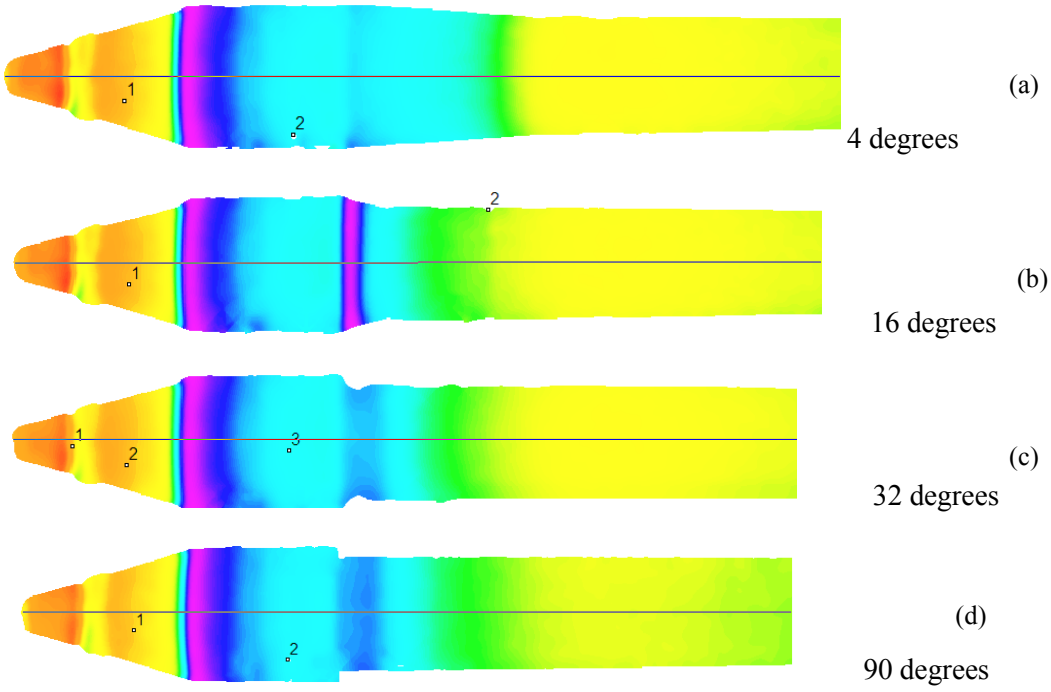

Fig. 17 PSP pressure field over the model for different values of boat tail angle.

Table 1 presents the main parameters observed in the pressure distribution along the model for Mach number 1.0. It is evident the highest gradients for the boat-tail angle of 16 degrees compared with the other geometries. It is also interesting observe that the boat-tail geometry that produced the lowest pressure gradients was the one with angle of 90 degrees.

Tab. 1 Main parameters observed in the pressure distribution along the model for Mach number 1.0

boat-tail angle	lowest pressure	lowest pressure after pay-load sector	highest pressure after pay-load sector	highest pressure in pay-load sector	greatest pressure ratio
4 degrees	19.9	30.4	48.0	34.1	2.41
16 degrees	18.1	18.7	47.1	32.7	2.60
32 degrees	18.8	27.4	44.7	31.8	2.38
90 degrees	21.0	29.0	46.8	34.0	2.22

Acknowledgments

The authors thanks FAPESP through the process 2013/23690-2, aimed at repairing the TTP compressor blades, CAPES trough Pró-estratégia project num. 20, 2011 and CNPq for the financial support through the processes: 560200/2010-2, 402233/2013-1 and 310646/2012-0 (first author).

References

[1] Azevedo, J L F, Moraes Jr., P, Maliska, C R, Marchi, C H, Silva, A FC (1996) Code validation for high-speed flow simulation over Satellite Launch Vehicle, *Journal of Space Craftand Rockets*, Vol. 33, No. 1, January-February.

[2] Moraes Jr., (2003) Ground and in-flight verification of the aerodynamic characteristics of the Brazilian Satellite Launch vehicle VLS

[3] Pirk, R., Desmer, W., Pluymers, B., Sas, P.,Goes, L C S (2002) Vibro-acoustic analysis of the Vehicle Satellite Launcher (VLS) fairing, In: Proceeding ISMA 2002, Vol. 5.

[4] Liu, T, Sullivan, J P (2005) Pressure And Temperature Sensitive Paints", Springer-Verlag, New York.

[5] Engler, R H, Klein, C, Trinks, O (2000) Pressure sensitive paint systems for pressure distribution measurements in wind tunnels and turbomachines, *Meas. Sci. Technol*., Vol. 11, 1077, doi:10.1088/0957-233/11/7/320.

[6] Gregory, J W., Asai, K, Kameda, M, Liu, T, Sullivan, J P (2008) A Review of Pressure Sensitive Paint for High Speed and Unsteady Aerodynamics", In: Proceedings of the Institution of Mechanical Engineers, Part G, Journal of Aerospace Engineering, Vol. 222, No. 2, pp. 249-980.

[7] Falcão Filho, J B P., Avelar, A C., Reis, M L C (2009) Historical Review and Future Perspectives For Pilot Transonic Wind Tunnel of IAE, *Journal of Aerospace Technology and Management*, Vol. 1, No. 1, pp. 19-27.

[8] Pope, A. and Goin, K. L., 1978, High-Speed Wind Tunnel Testing, John Wiley & Sons, Inc., New York, 474p.